Adaptation of Cross Entropy Optimisation to a Dynamic Bridge WIM Calibration Problem

Jason Dowling[1]*
Eugene J. OBrien[1]
Arturo González[1]

[1]*School of Architecture, Landscape and Civil Engineering, University College Dublin, Belfield, Dublin 4, Ireland*

*Corresponding Author. Tel.: +353 1 7163233; fax: +353 1 716 7399. *E-mail address: jasonkdowling@gmail.com*

Abstract

Moving Force Identification (MFI) theory can be used to create an algorithm for a Bridge Weigh-in-Motion (WIM) system that can produce complete force histories of the loads that have traversed a bridge structure. MFI is based on general inverse theory, however, and calibration of such a system requires a complete Finite Element (FE) model of the bridge to be available for implementation in the field. This is something that is often infeasible in practice as FE models created using theoretical values for material properties bear a poor relation to reality. The Cross-Entropy optimisation method has been adapted here to address this calibration problem. The general system FE global mass and stiffness matrices of the bridge FE model are found by best fit optimisation to match field measurements. In this fashion a fully automated calibration procedure is developed for an MFI algorithm. This system is tested theoretically using three different FE plate models, coupled with a three-dimensional vehicle model, allowing for Vehicle Bridge Interaction (VBI).

1 Introduction

Weigh-in-Motion (WIM) systems provide a means of gathering vehicle weight data without interruption to the flow of traffic. Bridge WIM uses an instrumented bridge as the vehicle weight sensor. Modern Bridge WIM systems [e.g., 1] can be installed and maintained without any interruption to the flow of traffic as there is no surface mounted instrumentation; both axle detection and strain measurement use gauges attached to the underside of the bridge. This is a significant advantage over alternative WIM technologies which require temporary lane closures for sensor installation or replacement.

Using gauges attached to the bridge soffit, Bridge WIM systems record strains as the vehicles traverse the bridge at normal highway speeds and from these calculate the static axle loads. Using bridges as weighing scales in this fashion was first proposed in the United States by Moses [2]. The algorithm presented by Moses sought to calculate the static loads traversing the bridge by minimising an objective function defined as the sum of the squared differences between static theoretical and measured strains. All commercial Bridge WIM systems known

to the authors still use algorithms based on static theory to calculate the static weights, attempting to minimise the effects of dynamics as Moses did, by using the many measurements available while the vehicle crosses the bridge. Dynamics – bridge vibration and vehicle/ axle motions – have been shown to be significant sources of error for Moses' algorithm [3], but are not considered in their algorithms.

In the field, theory can be a very poor descriptor of the bridge response unless the structure is calibrated. The theoretical response is described using an influence line, i.e., the static response of the bridge to a moving unit load. The calibration process of a Bridge WIM system involves determining the bridge's actual influence line, which can be quite a different shape than theory would suggest. There are different methods available to calibrate the influence line of a Bridge WIM system. McNulty and OBrien [4] adjust the influence line manually, point-by-point, until the response of the calibration vehicle(s) has/have satisfactorily been replicated. In their study, two different influence lines are calculated in this manner. In an alternative 'matrix' approach, OBrien et al. [5] calculate the influence line directly from measurements. This calibration procedure is similar to Bridge WIM, in that both are minimising the sum of the squares of the differences between theory and measurement, but Bridge WIM is solving for the axle weights given the influence line, whereas the matrix approach is looking for the influence line ordinates given the axle weights.

When dynamics is considered, Bridge WIM becomes an inverse structural dynamic problem, where applied axle forces are an unknown forcing function and they must be inferred from strain measurements and a theoretical bridge model. The solution of this ill-posed problem is ideally suited to dynamic programming and general inverse theory [6, 7]. Bridge WIM falls into a particular area of inverse dynamics known as Moving Force Identification (MFI). Indeed MFI theory represents an opportunity for Bridge WIM to predict axle weights much more accurately than has been previously possible.

MFI has received much attention in recent years. O'Connor and Chan [8] use an interpretive method, in which they calculate the dynamic loads directly from bridge strains, modelling the bridge deck as a series of massless beams connecting lumped masses. Law et al. [9] and Yu and Chan [10] later use a frequency time domain method, in which a Fourier transform is performed on the equation of motion, expressed in modal co-ordinates, and the force histories are found directly using the least squares method. Zhu and Law [11] utilise an orthogonal function method in the identification of moving loads. Law et al. [12] use a finite element method to identify the axle loads and a condensation technique to reduce the system to a smaller number of master degrees of freedom. For a more detailed review of the state of the art in MFI, see Yu et al. [13].

This paper utilises the first order regularisation method of MFI (as implemented by González et al. [14], Nordström [15], You et al. [16]), which is based in turn on the zeroth order MFI employed by Law and Fang [17]. This method utilises dynamic programming in combination with first order regularisation and the eigenvalue reduction technique, which reduces the

order of the system [18], to calculate the history of a number of vehicle forces from multiple strain measurements on the bridge. An unresolved problem for MFI algorithms in Bridge WIM is the MFI based algorithm's requirement for an accurate Finite Element (FE) model of the bridge. Similarly to Bridge WIM systems based on static theory, it is not possible to use theoretical FE models as, in the field, they often vary a great deal from measurement. A method is required, which uses the measured strain response of the bridge due to a truck of known weight, and infers from this the bridge mass and stiffness matrices. This paper addresses the issue of calibration using the Cross-Entropy (CE) method of optimisation [19] to calibrate the FE model used in the MFI algorithm. Measuring strains, the CE method infers the material properties required in order to build the system's mass and stiffness matrices, namely the material's flexural rigidities and densities. This removes the last practical obstacle to commercial implementation of MFI for Bridge WIM.

2 Numerical Vehicle-Bridge Interaction model

The numerical Vehicle Bridge Interaction model is comprised of a 3-dimensional sprung vehicle model coupled with a 2-dimensioal orthotropic FE plate model which allows for transverse effects and torsional modes of vibration. All numerical simulations are carried out in MatLab [20].

The bridge is modelled using thin plate elements [21] based on Kirchhoff plate bending theory. Each of the thin plate elements has 16 degrees of freedom, or four per node (vertical displacement, rotations about the X and Y axes, and the derivative of the vertical displacement with respect to the rotations about the axes). This differs from the standard Kirchhoff plate [21] in that there is one additional degree of freedom at each node. This derivative of rotation with respect to rotation can be called the nodal twist degree of freedom and is included to ensure continuity of slopes across element boundaries [22].

The vehicle is represented by sprung vehicle models as have been used by many researchers [e.g., 23-25]. The vehicle body is modelled as a lumped mass with three degrees of freedom: vertical displacement, pitch and roll. Each axle is modelled as a rigid bar with two lumped masses, representing the wheel assemblies, one at either end. Each wheel assembly has one, vertical displacement, degree of freedom. Spring-dashpot arrangements are included to model the vehicle suspension and tyres. The equation of motion for the vehicle is solved using the Newmark-β integration scheme [26].

Road surface roughness has long been known to be a dominant factor in influencing the dynamic response of a bridge to the passage of a vehicle [27]. Road surface roughness is therefore incorporated into the model in the form of a numerically generated surface profile. Carpet profiles are generated in the fashion of Cebon and Newland [28], using the inverse Fast Fourier Transform method. The profile used in this study is generated such that its properties are compliant with the ISO specifications [29]. A Moving Average Filter is applied to the road surface, prior to the calculation of the vehicle forces, to imitate the tyre contact

patch [30]. The roughness coefficient of the class 'C' profile which is used is 65×10^{-6} m^3/cycle.

The Vehicle-Bridge Interaction (VBI) problem is solved using an iterative procedure [24]. This procedure can briefly be described as follows. The wheel forces are calculated as the vehicle model travels over the road surface profile. These wheel forces are then applied to the bridge model and a vertical displacement of the bridge deck is calculated. The road surface profile is then updated to allow for the bridge deck displacements under it. The wheel forces are then calculated from this updated profile and the wheel forces applied to the bridge model again. The bridge deck displacement is then compared to that of the previous iteration and the process continued until convergence. The material properties required to be input to the FE model are the flexural stiffness in the longitudinal and transverse directions, and material density, for each plate element.

3 First order Moving Force Identification

The MFI method, based on the use of an FE model and an optimisation technique, is described in detail by González et al. [14]. Only those core features necessary for the explanation of the calibration method are reiterated here. This type of MFI algorithm is implemented in two stages: 1) formulation of equations of motion in state space suitable for dynamic programming and 2) Tikhonov regularisation and the L-curve method.

3.1 State space equations and dynamic programming

Firstly, the discretised equation of motion, shown in Equation 1 in time space, is reformulated into state space in Equation 2.

$$\mathbf{M}_{n\times n}\ddot{\mathbf{y}}_{n\times1}+\mathbf{C}_{n\times n}\dot{\mathbf{y}}_{n\times1}+\mathbf{K}_{n\times n}\mathbf{y}_{n\times1}=\mathbf{L}(t)_{n\times \mathrm{n_f}}\mathbf{f}(t)_{n_f\times1} \quad (1)$$

where **M**, **C** and **K** are the global mass, damping and stiffness matrices respectively; $\ddot{\mathbf{y}}$, $\dot{\mathbf{y}}$, and **y** are respective nodal accelerations, velocities and displacements; **L**(t) is a time-varying location matrix relating the external forces to the degrees of freedom; **f**(t) is the forcing function; n is the number of degrees of freedom and n_f is the number of external forces. The manipulation of Equation 1 to produce the final equation in state space includes an eigenvalue reduction technique [18] which reduces the computational demands of the calculations. In state space, the equation becomes:

$$\begin{Bmatrix}\mathbf{X}\\ \mathbf{f}\end{Bmatrix}_{i+1}=\mathbf{H}\begin{Bmatrix}\mathbf{X}\\ \mathbf{f}\end{Bmatrix}_{i}+\mathbf{T}\{\mathbf{r}\}_i \quad (2)$$

where **X** is a state vector of length 2n, containing the displacements and velocities of the degrees of freedom; **H** and **T** are system matrices obtained by manipulating eigenvectors and

natural frequencies and {**r**} is a vector containing the derivatives of the forces. Including the derivatives of the forces with the state variables produces a much smoother force prediction and a generally much better solution than the zeroth order approach [14].

The bridge response that is most readily measurable is strain and this is the response used throughout this study. To relate the measured strains to the state variables used in Equation 2, a selector matrix **Q** is used as in Equation 3.

$$\boldsymbol{\varepsilon}_{m\times 1} = \mathbf{Q}_{m\times 2n}\mathbf{X}_{2n\times 1} \tag{3}$$

where **ε** is the vector of recorded strain values and *m* is the number of simultaneous strain measurements. The **Q** matrix is utilized a great deal later in determining the material properties of individual plate elements.

3.2 Optimisation procedure

The second stage of the MFI approach involves the use of a numerical technique to improve the conditioning of the system. Tikhonov regularization [31] adds an optimum regularization parameter, λ, to the equations and solves a neighbouring and better conditioned problem. Hansen's L-Curve [32] is used to choose the optimum λ value. The method is described in detail by González et al. [14].

4 Calculating the Material Properties

The material properties required for an FE model of a bridge are the material density for each elemental mass matrix $\mathbf{M_e}$, and the material flexural rigidities (product of modulus of elasticity and second moment of area) for each elemental stiffness matrix $\mathbf{K_e}$. Walsh and González [33] propose the Cross-Entropy (CE) method of optimisation [19] in conjunction with static measurements to obtain the distribution of flexural stiffness within a 1-dimensional beam model. The CE method is applied here, with a novel objective function described in Section 4.1, and using dynamic measurements. Like the Genetic Algorithm [34] CE is a population based method of optimization. It can be described as an iterative procedure composed of two steps [35]; firstly a large portion of the population of solutions with high objective function values is culled; secondly, the remaining solutions are used to generate a new population. The CE method is used here to determine those global stiffness and mass matrices of the FE plate model that give a best fit of theoretical to measured strains for all runs of the pre-weighed calibration truck(s). The material properties that are needed, **η**, are each plate element's flexural stiffness and each plate element's mass per unit length.

The first step in the CE algorithm is to assume an initial statistical distribution of values of all elements of **η**. These distributions are taken to be Normal here and are therefore defined by means and standard deviations. The mean values can be based on typical theoretical values or

measurements on site. The efficiency of the method is not sensitive to the choice of standard deviations: values of 0.3 × mean have been used here for the initial population. A population of k trial $\boldsymbol{\eta}$ vectors are randomly generated using the initial mean and standard deviation. For each $\boldsymbol{\eta}$ in the population, strain measurements are calculated at a number of notional measurement locations on the bridge. There is a reduction in the sensitivity of the solution when there are fewer measurement locations considered in the problem.

The objective function is defined as the sum of the squared differences between the strains calculated for each trial FE model and the strains calculated for the actual FE model. The 'elite set' [19] retained to regenerate the population is defined as the 5% of trial bridges that give the lowest objective function values. With the mean and standard deviation of each component of this elite set, Monte Carlo simulation is used to generate the population for the next iteration of trial bridges. A tolerance is then specified to establish when convergence has been reached, in this case, 2.5% difference in successive objective function values.

A common problem with the CE algorithm is that it may converge prematurely to a false solution. Botev and Kroese [36] propose the method of 'injecting' extra variance into the samples to address this known problem. This technique simply involves increasing the value of the updated standard deviation between iterations. This 'widens' distributions at the start of the iterations, reducing premature convergence. This technique is implemented here by setting the standard deviation for the second iteration to 0.3 times the mean value, and reducing this incrementally over the next number of convergences. The mean value for this second iteration is the mean of the elite set obtained in the previous iteration. The number of convergences specified for each problem varies according to the complexity of the problem, examples are shown in Section 5. The number of convergences specified before the solution is deemed final, varies depending on the complexity of the problem.

4.1 Optimisation and the Objective Function

Least squares fitting problems are common in Engineering. Some of these problems may be referred to as "Linear Combination" (LC) problems, i.e., optimisation problems for which the objective function is a sum of univariate functions: $O = \sum_{i=1}^{m} O_i = \sum_{i=1}^{m} f_i(x_i)$, where f_i are functions (often quadratic) and x_i; i = 1:m, are the parameters whose values are sought. Other Engineering optimisations are referred to here as "Near Linear Combination" (NLC). The objective function in an NLC problem is again a linear combination of objective sub-functions, O_i, but this time, there is not necessarily a direct mapping from the variables to the sub-functions. The definitive property of an NLC problem is that the sub-functions are each sensitive to small groups of variables and are insensitive to all others. This can be expressed as:

$$\frac{\Delta O_i}{\Delta x_j} = \begin{cases} \text{large where } O_i \text{ and } x_j \text{ are neighbours} \\ \text{small otherwise} \end{cases}$$

NLC problems are characterised by optimum x_i being largely independent of the values of x_j, where i and j are not neighbours – see for example Figure 1(a) – the optimum value for x_2 is substantially independent of x_1, i.e., $\hat{x}_2(x_1 = a) \approx \hat{x}_2(x_1 = b)$. This is not the case for a non-NLC problem – Figure 1(b) – $\hat{x}_2(x_1 = a) \neq \hat{x}_2(x_1 = b)$.

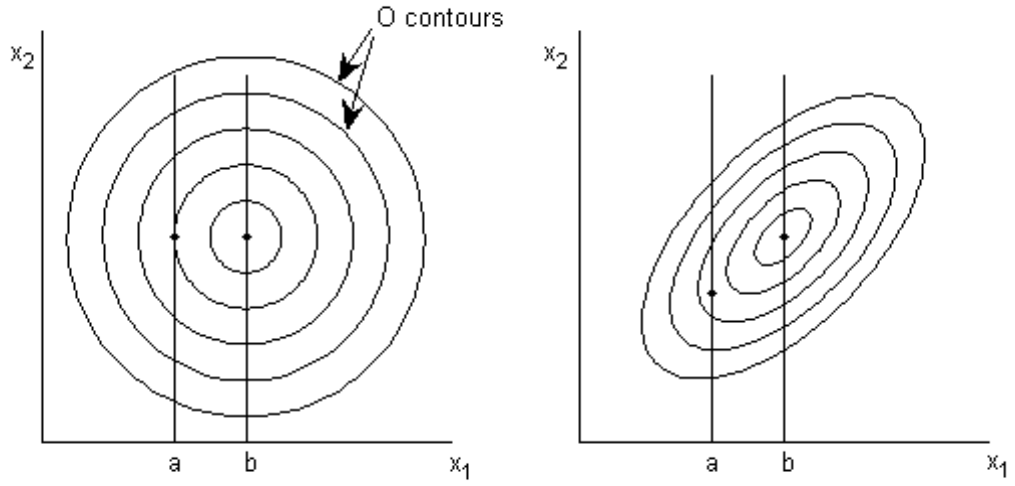

(a) NLC problem where x_1 and x_2 are not neighbours

(b) Non-NLC problem

Figure 1 Objective function contours

NLC problems can be solved using conventional CE but convergence is slow due to the high dimensionality (no. of variables). By sub-structuring, these problems can readily be reduced to a series of much simpler low dimensional sub-problems.

Conventional CE uses the global objective function, *O*, to identify the elite set of trial solutions, i.e., those corresponding to minimal *O* values. A matrix of *n* trial values of *m* parameters is illustrated in Figure 2. In this matrix the trial solutions are ranked in order of increasing objective function, O^j, and the top *p* solutions are defined as the elite set. This elite set is used to create the next generation of trial solutions. For example, for parameter 2, the mean and standard deviation of its values in the elite set, x_2^i, i = 1:*p*, are used to generate its values in the next set of trials.

For a sub-structurable problem, an alternative approach is more computationally efficient. For each trial solution, all of the objective sub-functions are evaluated as shown in Figure 3. For each parameter x_i, the objective sub-functions are identified that are neighbours to that parameter, i.e., j for which $\frac{\Delta O_j}{\Delta x_i}$ is not small. Some parameters may have few neighbours while others may have many. In the example of Figure 3, O_3 and O_5 are identified as neighbours of x_2. The objective sub-functions are ranked and the trial numbers corresponding to the *p* least values identified. In this example, trials 1, 2 and 5 are optimal for O_3 and trials 2, 3 and 5 for O_5. The optimal trials are merged, giving a combined elite set of trials 1, 2, 3 and 5. The

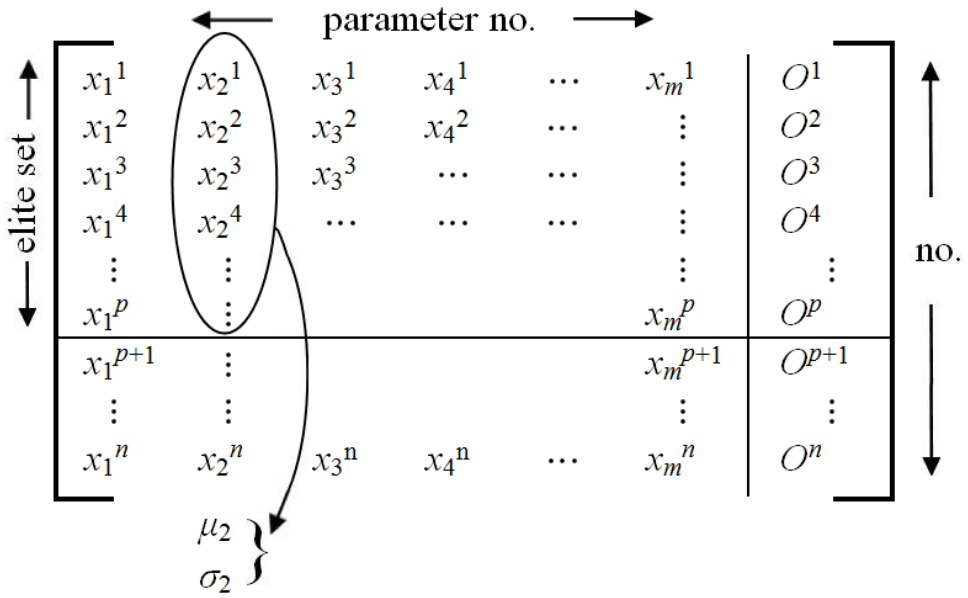

Figure 2 Conventional CE elite set (μ_2 and σ_2 are the mean and standard deviation of the elite set for x_2)

mean and standard deviation of this combined set are used to create the next generation of trial values for x_2. This is different from conventional CE in that the trial values of each component are generated independently of most of the others. This approach is valid provided the problem is sub-structurable, e.g., provided the optimum value of x_2 is substantially independent of all other parameters.

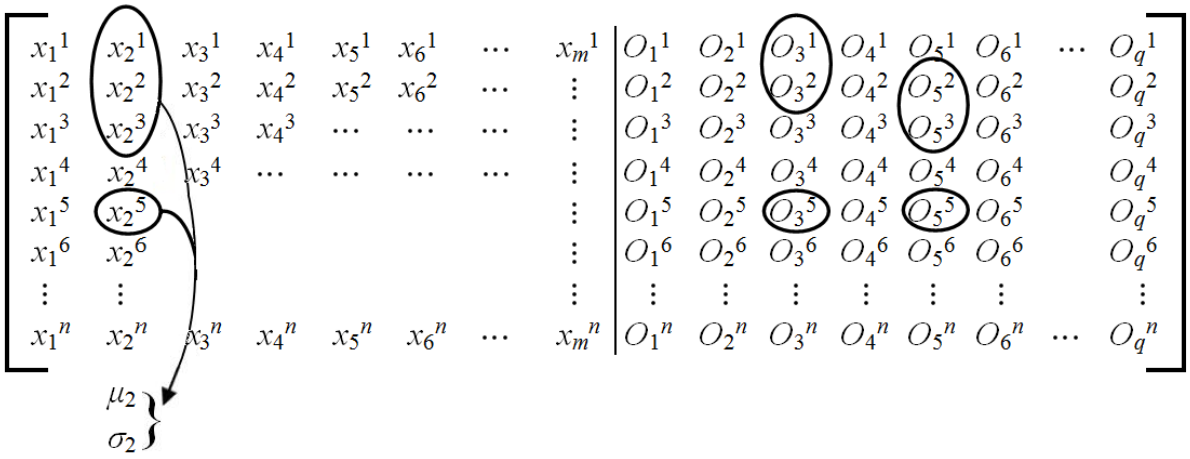

Figure 3 Selecting mean and standard deviations for x_2 using the new approach

5 The Calibration of Finite Element models

The algorithm is tested using three different FE model configurations to demonstrate robustness. The first configuration is a 12m long, by 8m wide simply supported bridge, discretised into 1m × 1m plate elements, each with identical properties. This first, and simplest case, is treated as an example procedure, showing clearly all of the steps involved.

The second example is also a 12m long, by 8m wide simply-supported bridge, but in these simulations the bridge is discretised into sixteen 3m × 2m plate elements, each with their own material properties. Lastly, Section 5.4 presents the calibration of a beam and slab bridge based on an existing bridge in Slovenia.

5.1 Plate elements with identical properties throughout

Figure 4 shows the FE model used for the case of plate elements with identical material properties.

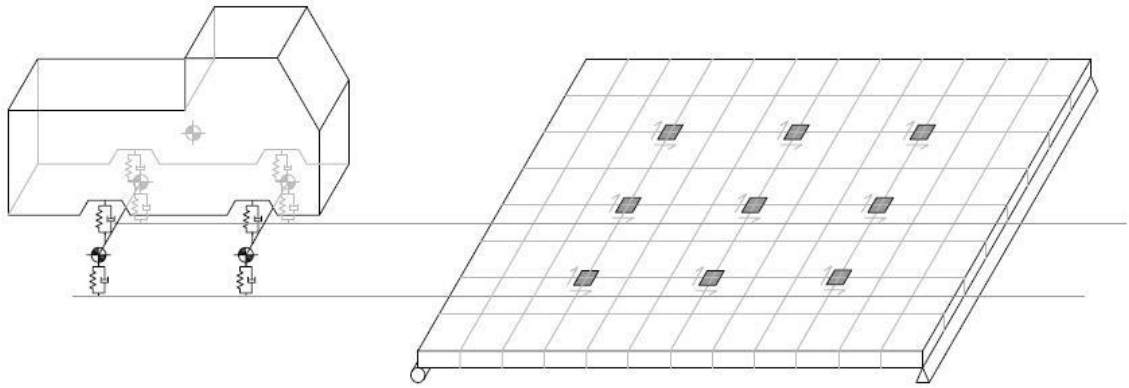

Figure 4 Schematic of 8m by 12m bridge model and 2-axle calibration truck

The 2-axle vehicle, also shown in the figure, has an axle spacing of 5.5m; first and second axle weights of 59.5kN and 108.6kN respectively and velocity of 20m/s. Typical values from the literature [37] are taken for tyre and suspension properties.

Figure 4 also shows the locations of the sensors used to gather the strain data. There are nine locations in this example (and again in the next example in Section 5.3), where both longitudinal and transverse strains are recorded: ¼-span, mid-span and ¾-span in the longitudinal direction and 2m, 4m and 6m in from the right-hand side in the transverse direction.

Steps in procedure:

1) Record both longitudinal and transverse strains during the entire passage of the calibration vehicle (of known characteristics).
2) Initial estimates of the values being sought are required to be input to the system to create the first generation of trial solutions. Values with an error of ±30% were typically used. The solution was found to be insensitive to the initial values input.
3) The global stiffness matrix, $\mathbf{K}$ is assembled using the elemental stiffness matrices, $\mathbf{K_e}$ of each plate element. The error function used in the CE method is defined as the sum of the squared differences between the measured strains and the simulated static strains using the longitudinal and transverse stiffness estimates. For the static strain calculations, the equation of motion of Equation 1 is used with the mass and damping matrices set to zero.

4) Using the **K** matrix calculated in 3), $\mathbf{M_e}$ is calculated for each plate element, taking the error function to be the sum of the squared differences between the complete measured strains and the simulated total strains using the mass per unit length estimates. The global mass matrix, **M** is assembled from the individual $\mathbf{M_e}$ matrices.

The introduction of step 3) reduces, initially, the number of unknowns in the problem by two-thirds. I.e. the mass component of the equation of motion is not considered at the third stage, calculating **K** with a pseudo-static equation of motion considering only two of the three unknowns for each element, those relating the longitudinal and transverse flexural stiffness. The remaining unknown, the mass per unit length, is then considered in step 4). This decoupling of the problem has been found to greatly improve efficiency.

In this first example, it is assumed that the material properties of all the plate elements are identical and hence, only three parameters are sought, the flexural stiffness in the longitudinal direction EI_{xx}, the flexural stiffness in the transverse direction EI_{yy} and the plate element mass per unit length μ. The values used to generate the 'measured' data are $35 \times 10^9 \text{Nm}^2$ for EI_{xx} and EI_{yy} and 1,560kg/m for μ.

Figure 5 presents three target (theoretical) longitudinal strains, for illustrative purposes, from virtual sensors located at ¼-span, mid-span and ¾-span along the central spine of the bridge. The influence of measurement noise will be investigated in Section 5.2.

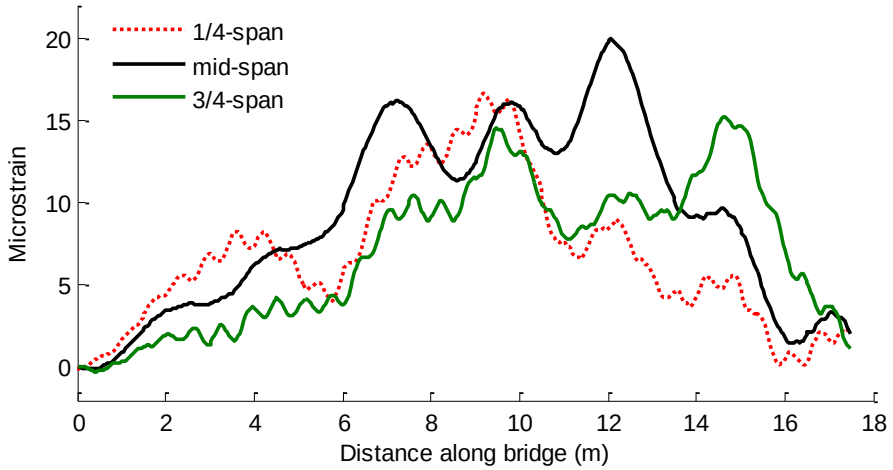

Figure 5 Longitudinal target strains for three sensor locations

The progression of the CE method can be seen in Figure 6, which shows the convergence of EI_{xx} values towards the correct solution. The vertical lines of dots in the figure are the trial EI_{xx} estimates. These dots are located at each iteration, and are so closely spaced vertically, that they in some places appear to be a vertical line. From the second iteration onwards, the standard deviation of the elite set is artificially inflated using the method proposed by Botev and Kroese [36], of 'injecting' extra variance into the samples, to prevent premature convergence. This method has been described previously in Section 4. In this particular example, the correct solution is very quickly found. Injection is applied, despite not being

required, for illustrative purposes, and the steady reduction in standard deviation from iteration number 2 onwards can be seen in the figure.

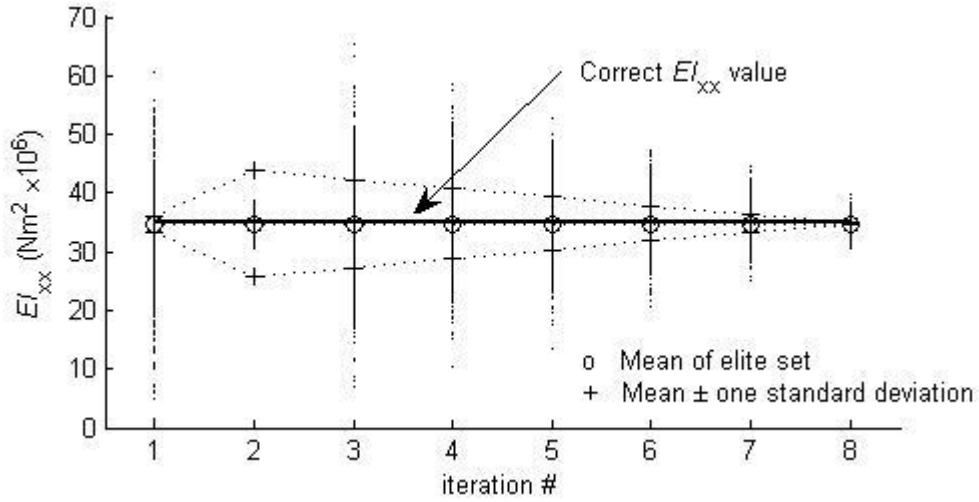

Figure 6 Progression of EI_{xx} values through eight iterations of the CE algorithm

The final EI_{xx} value inferred by the algorithm is not necessarily the mean value of the final iteration, but rather the value which gives the lowest error function value from the entire simulation. The progression of the EI_{yy} and μ values is similar to that of the EI_{xx} values. The final EI_{xx} and EI_{yy} values are 34.79×10^9Nm^2 and 34.94×10^9Nm^2, giving errors of -0.60% and -0.17% respectively. The final μ value is 1,552kg/m, corresponding to an error of -0.54%.

The next stage is the application of the MFI algorithm using the **M** and **K** matrices determined from the imperfect calibration procedure. The sensor locations used for the MFI algorithm are the same as for the calibration procedure, but only longitudinal and not transverse strains, are used. The L-Curve method of selecting the optimum regularisation parameter is presented in Figure 7. The optimum regularisation parameter is the point of maximum curvature on the L-Curve as defined by Busby and Trujillo [32], or the point of maximum positive curvature in Figure 7(b).

Using the optimum regularisation value of $\lambda = 2 \times 10^{-18}$, the wheel forces are predicted. Figure 8 shows the actual and predicted forces for the sum of the left and right wheels of each of the first and second axles to give the total forces for each axle.

The predicted forces are in good agreement with the actual values for large portions of the force histories, for both the MFI algorithm calibrated using the CE method and for the MFI algorithm using the exact **M** and **K** matrices. The predictions using the **M** and **K** matrices calculated with the CE method, are almost identical to those calculated using the exact **M** and **K** matrices (the differences are barely visible in the figure).

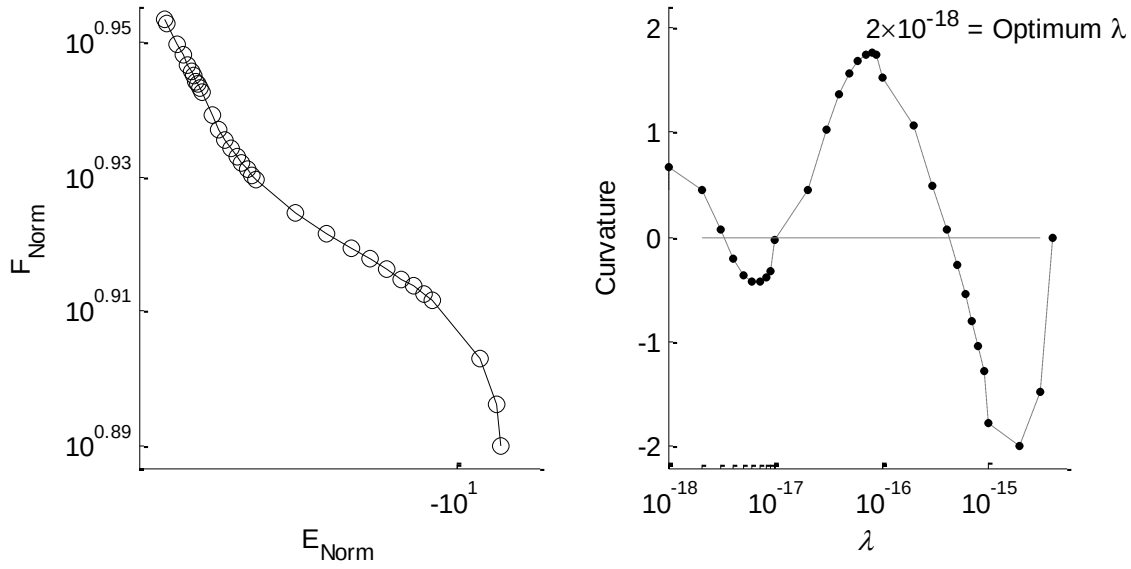

(a) L-Curve for λ values between 9×10^{-19} and 4×10^{-15}

(b) Curvature

Figure 7 Selecting the optimum regularisation parameter

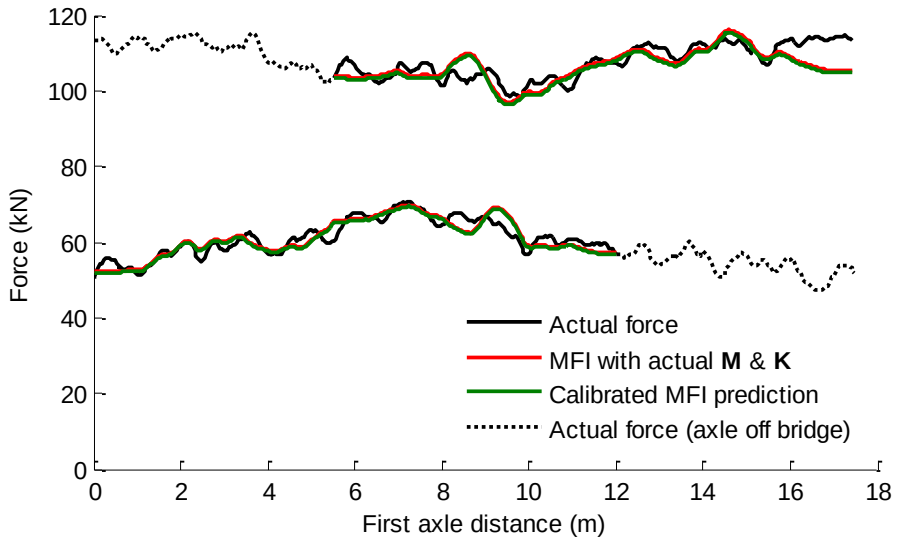

Figure 8 Axle forces predicted using the MFI calibrated with the CE method

The road used in this example is a class 'C' profile so as to induce relatively large excitation forces in the wheels of the vehicle. This was done to highlight the capabilities of the MFI algorithm, but also to show that the CE method of calibrating the MFI algorithm is capable of dealing with strain signals with high levels of dynamics present.

5.2 The Influence of Noise

Measurement noise is often quite inescapable when theoretical work is tested experimentally onsite. To demonstrate the ability of the method presented here to deal effectively with noise, simulations are presented here containing measurement noise of varying levels. Gaussian noise is added to the simulated strains, specified as a percentage of the maximum strain. That is, the theoretical strain is polluted with normally distributed random noise, of zero mean and standard deviation of one times a specified percentage of the maximum strain induced due to passage of the vehicle forces. The levels considered were 1%, 2%, 3%, 4%, 5%, 10%, 15% and 20%. Four of these levels are depicted in Figure 9, for the case of the central of the three mid-span sensors.

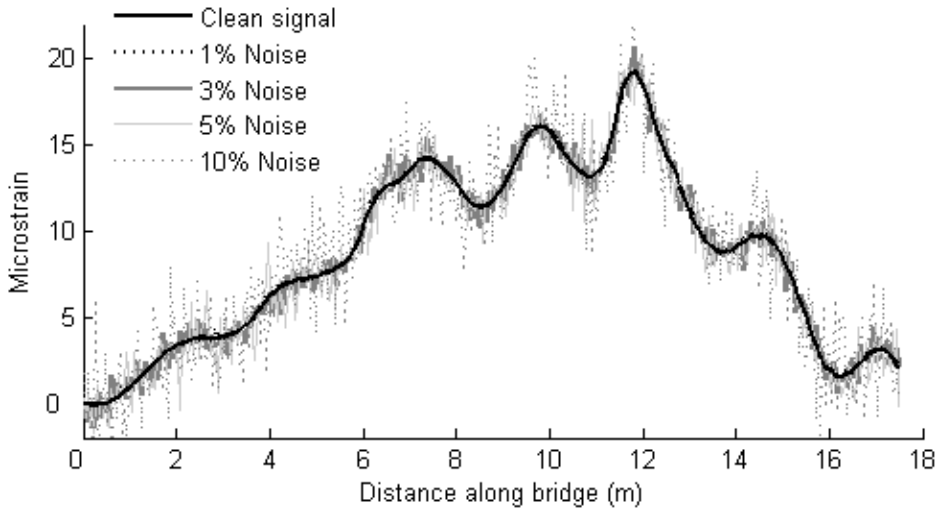

Figure 9 Gaussian noise of 1%, 3%, 5%, and 10%

The CE method described in Section 5.1 is repeated for the eight cases of the input strains contaminated with Gaussian noise. The percentage errors in the calculated material properties for the simulations are presented in Figure 10.

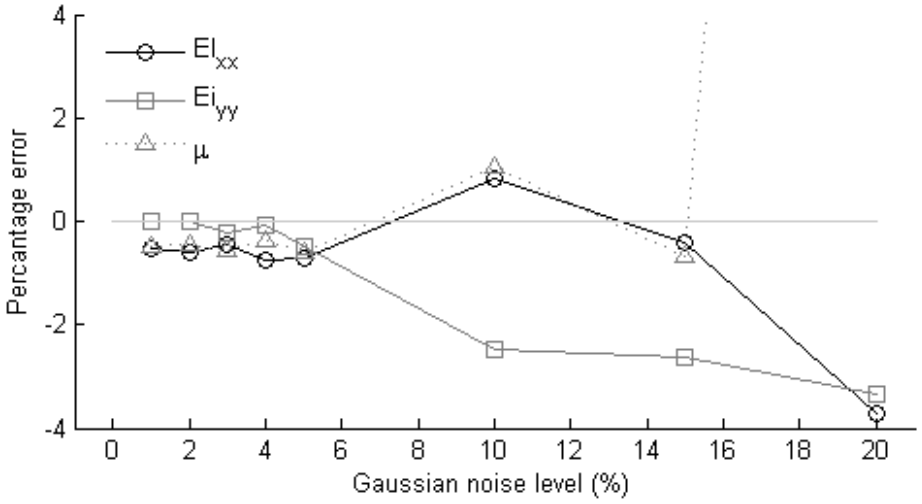

Figure 10 Percentage errors in the calculated material properties

The errors for the cases of noise levels up to 5% of the maximum strain are all less than 1%. More significant errors are noticed for noise levels of 10% of the maximum strain and higher. The error in the calculated μ value for the case of noise level of 20% of the maximum strain was 42%. The proposed method seems robust for levels of noise of 5% of the maximum strain or less.

5.3 Sixteen plate elements

The CE algorithm is used here to calibrate FE models with non-uniform EI_{xx} and EI_{yy} values throughout the bridge. Permitting so much variation in the modelled system presents an adaptable method of calibrating the algorithm that can allow for slight variations within the materials in the longitudinal or transverse directions, or local concentrations of stiffness due to haunches, etc.. Increasing the complexity of the problem significantly in this way, requires an increased number of measurement locations. The FE model used in this section is a 12m × 8m, simply-supported bridge discretised into sixteen 3m × 2m plate elements. The 2-axle vehicle velocities are all in the range of 20 - 25m/s.

Sub-structuring of problem

The FE grid for the bridge has a node at each of the measurement points, the same locations as in the example in Section 5.1. The objective function is the sum of squared differences between theoretical and measured strains at the measurement points. Hence, when sub-structured, the number of objective sub-functions is equal to the number of measurement points. As measured strains are constant, this is a linear combination of quadratic functions of the theoretical strains at the measurement nodes. Figure 11 shows four plate elements and their associated nodes. The strain at the measurement point, node 5, is a function of the displacements at the four corners of each of the adjacent elements. The problem is assumed to be Near Linear Combination with neighbouring variables being defined as those associated with elements touching the same measurement point. It is implicit in this assumption that the strain at node 5 is strongly influenced by the properties of the four adjacent elements, p1 through p4, and is less influenced by the properties of other elements in the mesh.

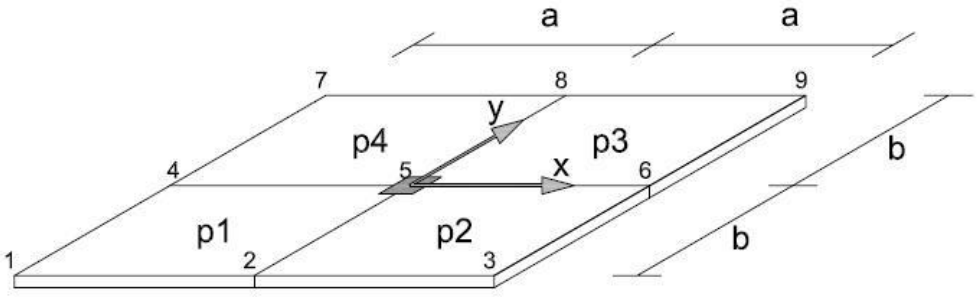

Figure 11 Relating a single measurement location to four plate elements

Results

Six bridges are considered, with assumed differences of properties between plate elements. The EI_{xx} and EI_{yy} values are assigned to each element by randomly sampling values from a Normal distribution with varying standard deviations. The values of μ are kept constant for all six bridges. There are configurations of stiffness profiles, ranging from constant flexural stiffness, as in the case of the simulation of Section 5.1, to randomly varying flexural stiffness with a standard deviation of 25% in values. The longitudinal flexural stiffnesses for element numbers 1 through 16, are shown in Figure 12 (indicative of the transverse profiles also).

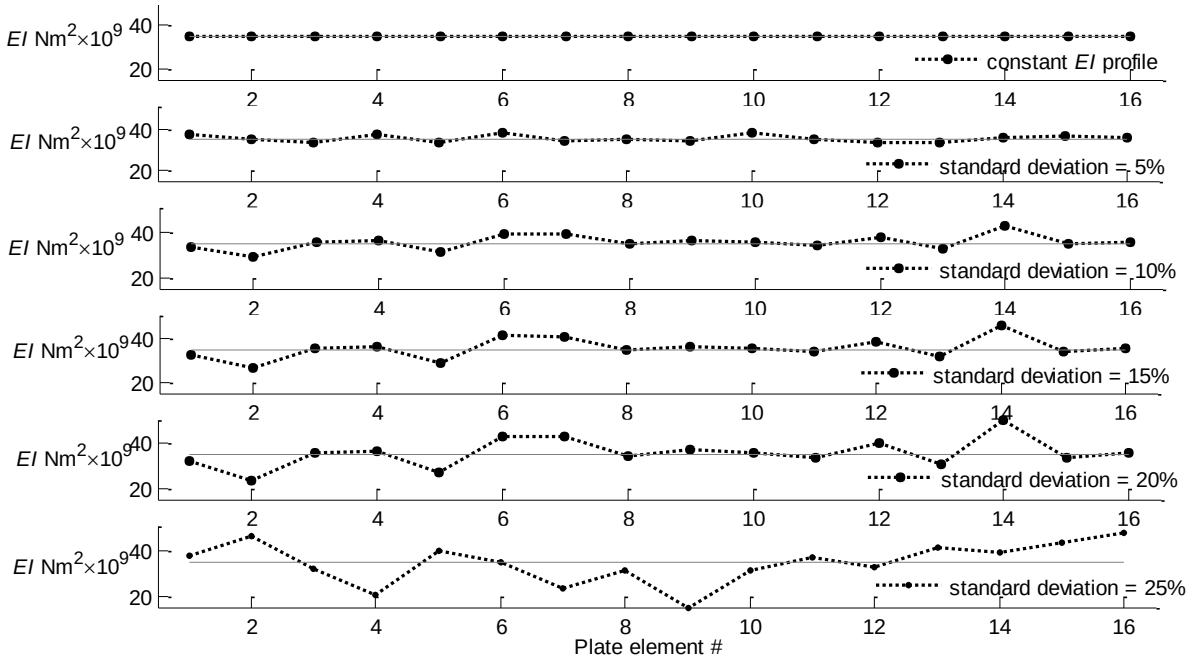

Figure 12 The six EI_{xx} profiles used (indicative of the EI_{yy} profiles also)

Figure 13 shows the results of applying the CE method to the second of the six bridges (varying EI_{xx} profile with a standard deviation of 5% of mean value). The predictions of Figure 13 are very good, with an average error of 1.0%. Figure 14 shows the predicted forces of the calibration truck on the bridge using the inferred EI_{xx} values.

The calculated forces using the 48-variable optimisation problem (16 elements, with three unknowns for each: EI_{xx}, EI_{yy} and μ), are a good fit to the actual axle forces except near the points where axles arrive and depart from the bridge. This phenomenon has been documented as a weakness of MFI previously [14], as a result of the small contribution to the total strain of the entering/ exiting wheels. The problem has been re-run assuming all elements to have equal properties. This gives reasonable, though less accurate, results. It would seem a good approximation for bridges with modest variations in properties.

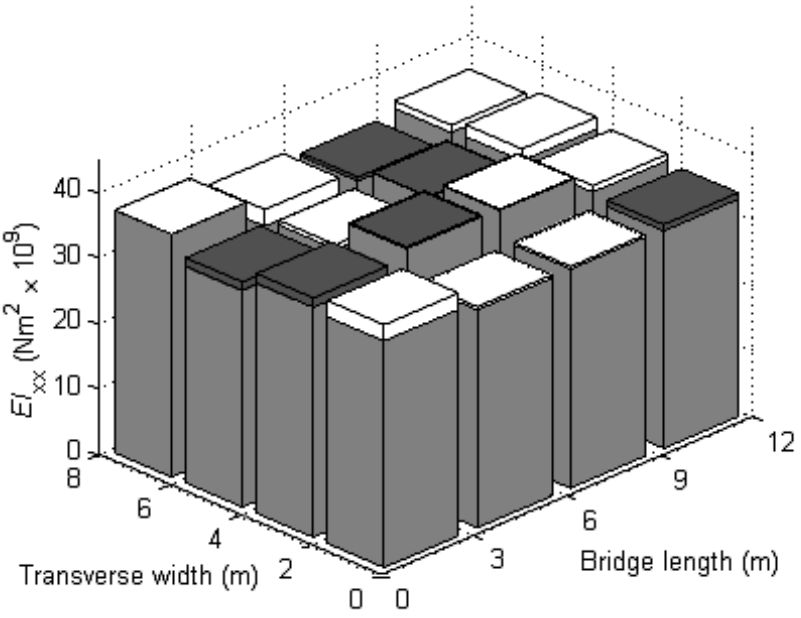

(a) By location (white = under-estimation; black = over-estimation)

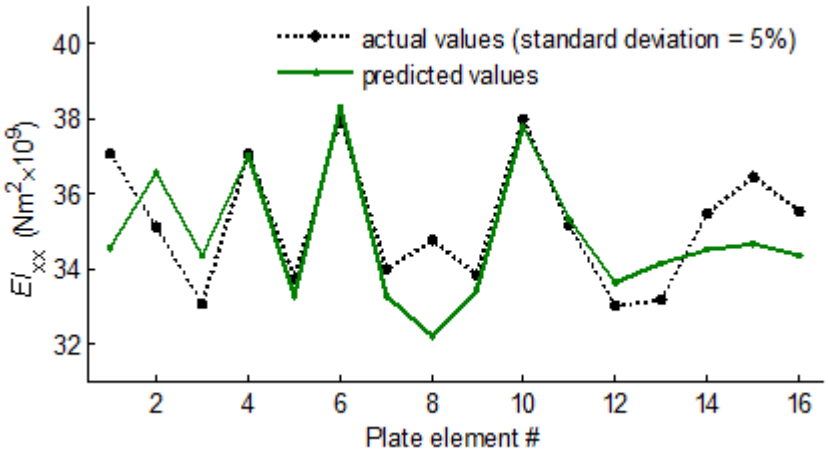

(b) By element number

Figure 13 Final EI_{xx} predictions from 48 variable optimisation problem, for a varying EI_{xx} profile (5% standard deviation)

The results for all six bridges are shown in Table 1. The measure of accuracy used is a simple sum of the squares of the differences between the true force and the calculated force. The first and last 10% of predicted force histories were discounted in these accuracy calculations. Unsurprisingly, the assumption of constant stiffness for all elements results in significant errors as the true variation of stiffness in the bridges increases. The 48-variable optimisation problem works well for all six bridges and gives consistent levels of accuracy. This is illustrated in Figure 15.

Table 1 Sum of the squares of the differences between the actual wheel forces and those calculated using the calibrated MFI algorithm (central 80% of results)

	Bridge number					
	# 1	# 2	# 3	# 4	# 5	# 6
Assuming 48 unknowns						
1st axle, left	9.5	11.8	6.4	11.0	8.2	14.5
1st axle, right	7.8	12.0	6.0	10.9	8.1	14.5
2nd axle, left	3.2	10.0	2.9	6.9	4.6	14.3
2nd axle, right	5.6	14.5	3.9	7.7	5.2	14.2
Average error	6.5	12.1	4.8	9.1	6.5	14.4
Assuming all elements identical (3 unknowns)						
1st axle, left	7.5	24.4	13.8	27.8	49.9	79.3
1st axle, right	6.6	21.1	13.4	29.3	52.1	83.4
2nd axle, left	3.1	34.3	27.3	54.0	90.1	136.9
2nd axle, right	2.9	19.0	24.6	52.2	90.0	137.9
Average error	5.0	24.7	19.8	40.8	70.5	109.4

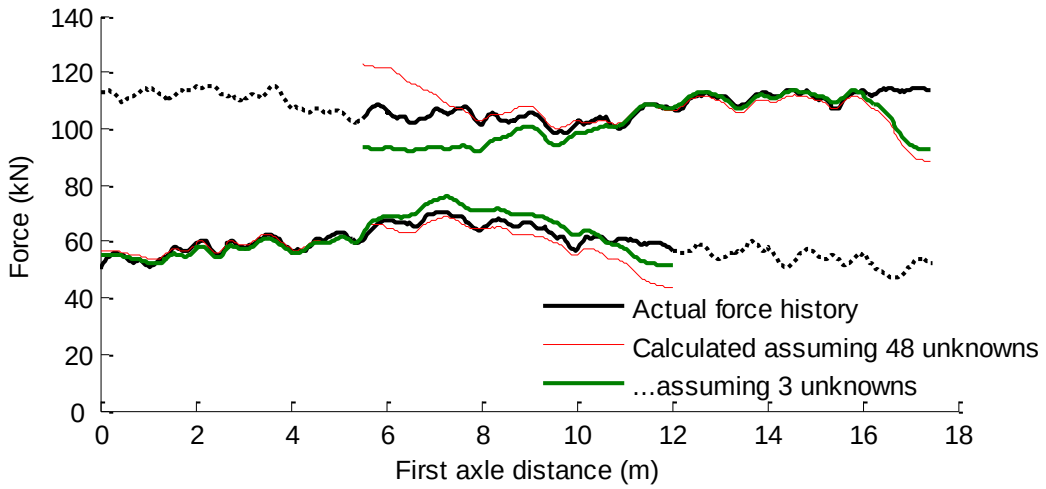

Figure 14 Comparing the forces calculated using two CE calibration algorithms for a varying EI_{xx} profile (5% standard deviation)

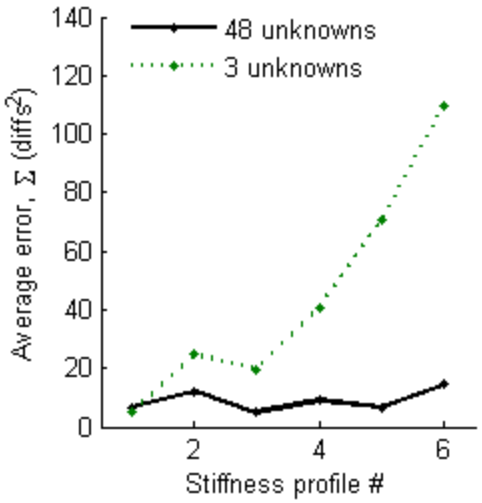

Figure 15 Errors for the two calibration procedures

5.4 A Beam and Slab bridge model

A more complex bridge geometry is also considered. This is a beam and slab (girder) bridge based on an existing 24.8m × 12.07m, simply-supported structure located at Vransko in Slovenia [38]. Figure 16 shows a transverse section through the bridge.

The FE model of the bridge at Vransko is discretised into 100 plate elements (10 × 10). All elements in the longitudinal direction are 2.48m long, while in the transverse direction, two plate elements are placed between each beam and one outside each outer beam. The girders

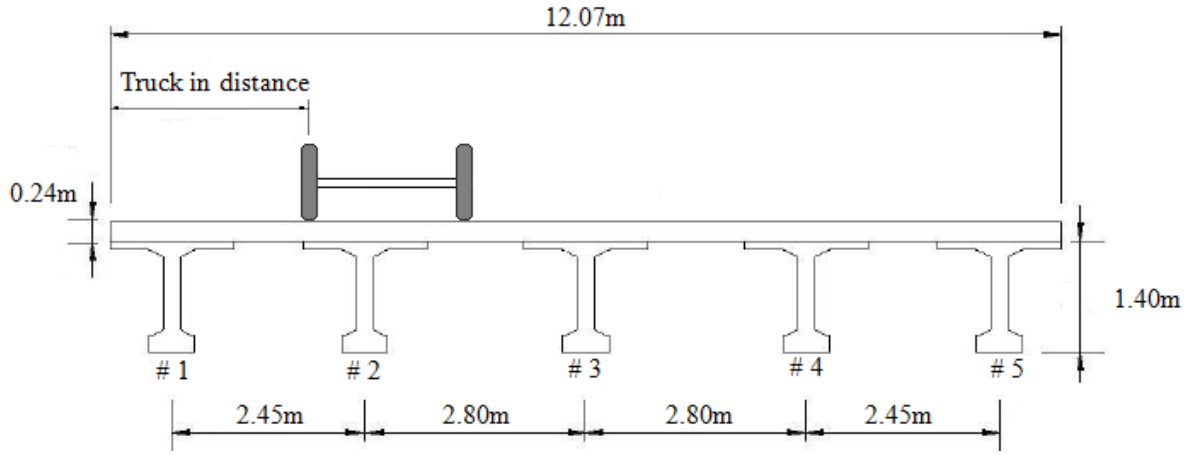

Figure 16 Section through the bridge at Vransko

are modelled as six degree of freedom beam elements, adding additional stiffness along rows of nodes corresponding to beam locations. For the nodes which are beam locations, the properties of the combined beam and the width of slab above it, are calculated relative to the centroidal axis of the combined section [39], to account for the extra stiffness in the beams due to the width the slab above it. There are more measurement locations considered in this

example. Again, there are three longitudinal locations, at the fourth, sixth and eighth nodes from the left hand support (7.44m, 12.4m, 17.36m from the laft hand support). In the transverse direction, the centre of each beam and the slab between each beam are also taken as measurement locations. This gives a total of 27 measurement locations in this case. The material properties found in a previous study [40] to best model the bridge at Vransko are listed in Table 2. Figure 17 gives an example of the strain responses from the beam and slab model, for the case of the same 2-axle truck as before, travelling at a velocity of 20m/s.

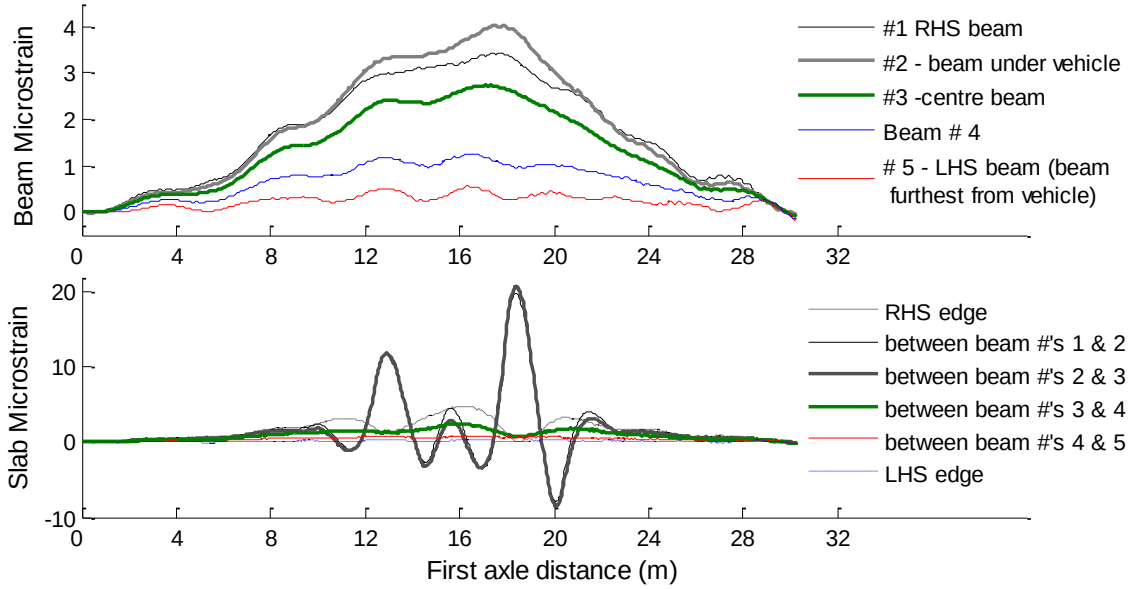

Figure 17 Strain responses from beam and slab FE model

The CE algorithm is applied to find the material properties of the slab (EI_{xx}, EI_{yy} and μ) and the beams (EI_{xx}^{b} and μ^{b}). The results are summarised in Table 2, showing very close agreement with the previous study.

Table 2 Results of the CE algorithm applied to the beam and slab FE model (μ represents the mass per unit (longitudinal) length of a plate element 1m long in the transverse direction)

	Rowley et al. [37]	CE calculated
EI_{xx} (Nm^2)	31.0×10^9	31.3×10^9
EI_{yy} (Nm^2)	31.0×10^9	30.9×10^9
μ (kg/m)	576	577
EI_{xx}^{beam} (Nm^2)	35×10^9	34.8×10^9
μ^{beam} (kg/m)	1,373	1,358

Figure 18 presents the convergence, through the iterations of the CE method, of the μ value for the slab. The simulation converged a total of three times, at iteration numbers 4, 12 and 18, before the objective function value was deemed sufficiently low to end the process.

Artificial inflation of the standard deviation of the population solutions was applied at iteration numbers 4 and 12, where the artificially high standard deviation value can be seen despite the scatter of the trial values being very small (all contained within the circular mean marker).

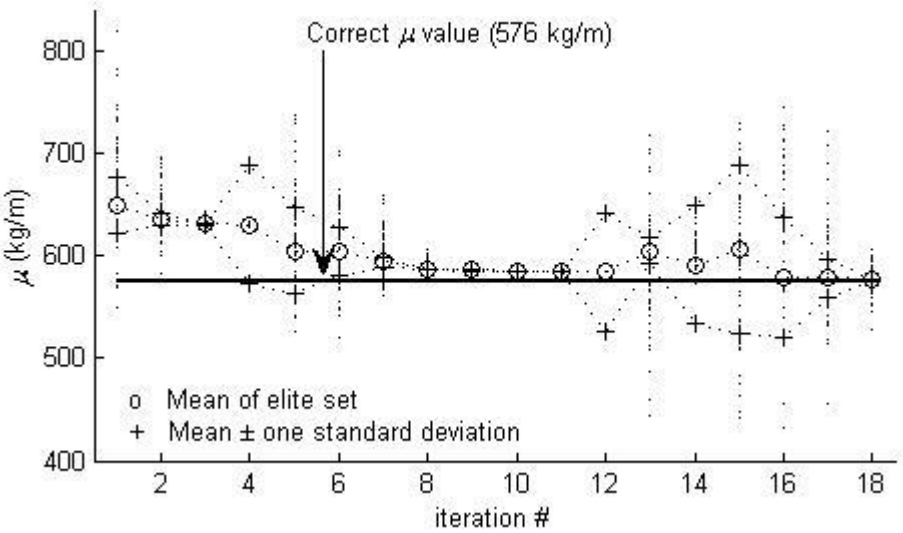

Figure 18 Convergence of CE method for the μ parameter

Figure 19 shows the effect of the CE calibration procedure on the forces predicted. There is a particularly high level of dynamics evident in the axle forces as a class 'C' road profile is used. The calibrated MFI algorithm tracks the forces reasonably well and captures two significant frequencies in the applied force signal, at frequencies of approximately 1.2 and 14.3Hz.

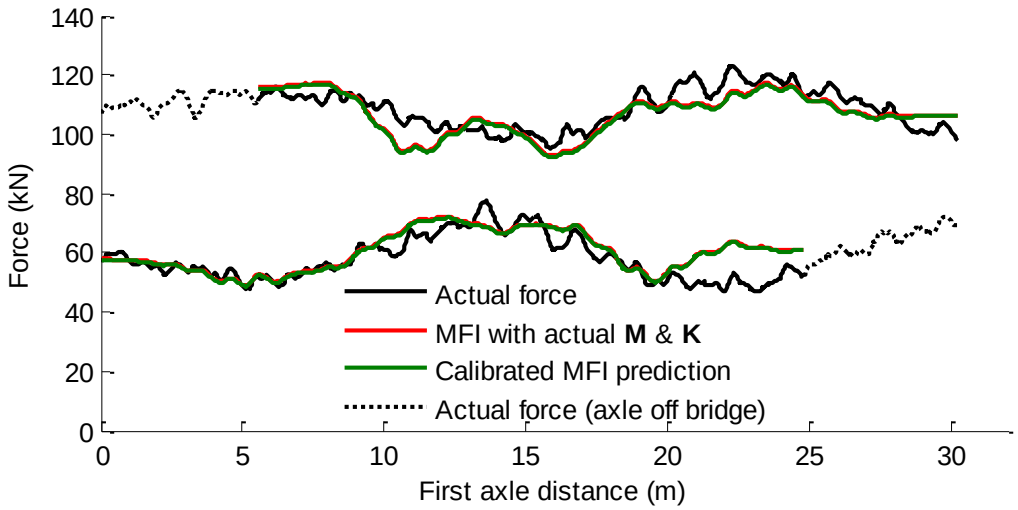

Figure 19 Comparing the forces calculated using the Exact system matrices and those calculated using CE calibration algorithm

The calculated forces using the mass and stiffness matrices inferred by the CE algorithm almost exactly match those forces calculated using the values used to simulate the data. (They

are such a close match that it is difficult to distinguish the two sets of calculated force lines in Figure 19). This is unsurprising, considering the high levels of accuracy achieved in the results in Table 2.

6 Conclusions

It seems likely that MFI based algorithms will be at the core of future Bridge WIM systems. The MFI requirement of an accurate FE model of the bridge, provided a challenge to its integration with Bridge WIM systems. This paper has shown that the Cross Entropy optimisation method can be used successfully to calibrate the system matrices required of the MFI algorithms, removing the final obstacle to their implementation. The multi-dimensional optimisation problem is sub-structured, greatly improving its numerical efficiency. Three FE models are successfully calibrated taking strain as input, and the effect of the calibration procedure is seen in the force history predictions of the MFI algorithm.

References

[1] Žnidarič, A., Lavrič, I. and Kalin, J. (2002). The Next Generation of Bridge Weigh-in-Motion Systems. In: Jacob, B. and OBrien, E.J. (Eds.), *Proceedings of Third International Conference on Weigh-In-Motion (ICWIM3)*, Orlando, FL, USA, 219-29.

[2] Moses, F. (1979). Weigh-In-Motion System using Instrumented Bridges. *ASCE Journal of Transportation Engineering*, **105**(3): 233-49.

[3] OBrien, E.J., Žnidarič, A. and Dempsey, A.T. (1999). Comparison of two independently developed bridge weigh-in-motion systems. *Heavy Vehicle Systems, International Journal of Vehicle Design*, **6**(1/4): 147-61.

[4] McNulty, P. and OBrien, E.J. (2003). Testing of a bridge weigh-in-motion system in cold environmental conditions. *ASME Journal of Evaluation and Testing*, **31**(6): 497-506.

[5] OBrien, E.J., Quilligan, M. and Karoumi, R. (2006b). Calculating an Influence Line from Direct Measurements. *Proceedings of the Institution of Civil Engineers: Bridge Engineering*, **159**(BEI): 31-4.

[6] Trujillo, D.M. (1975). The direct numerical integration of linear matrix differential equations using Padé approximations. *International Journal for Numerical Methods in Engineering*, **9**(2): 259-70.

[7] Trujillo, D.M. and Busby, H.R. (1997). *Practical inverse analysis in engineering*, CRC Press, Boca Raton, FL, USA.

[8] O'Connor, C. and Chan, T.H.T. (1988). Dynamic wheel loads from bridge strains. *ASCE Journal of Structural Engineering*, **114**(8): 1703-23.

[9] Law, S.S., Chan, T.H.T. and Zeng, Q.H. (1999). Moving force identification: a frequency and time domain analysis. *ASME Journal of Dynamic systems, Measurement and Control*, **12**: 394-401.

[10] Yu, L. and Chan, T.H.T. (2003). Moving force identification based on the frequency-time domain method. *Journal of Sound and Vibration*, **261**: 329-49.

[11] Zhu, X.Q. and Law, S.S. (2001). Orthogonal function in moving loads identification on a multi-span bridge. *Journal of Sound and Vibration*, **245**(2): 329-45.

[12] Law, S.S., Bu, J.Q., Zhu, X.Q. and Chan, S.L. (2004). Vehicle axle loads identification using finite element method. *Engineering Structures*, **26**: 1143-53.

[13] Yu, L., Chan, T.H.T. and Xu, D. (2005). Moving Force Identification: Practice and Review. In: OBrien, E.J., Jacob, B., González, A., and Chou, C-P. (Eds.), *Proceedings of 4th International Conference on Weigh-in-Motion (ICWIM4)*, Taipei, Taiwan, 118-27.

[14] González, A., Rowley, C. and OBrien, E.J. (2008b). A general solution to the identification of moving vehicle forces on a bridge. *International Journal of Numerical Methods in Engineering*, **75**(3): 335-54.

[15] Nordström, L.J.L. (2006). A dynamic programming algorithm for input estimation on linear time-variant systems. *Computer Methods in Applied Mechanics and Engineering*, **195**(44-47): 6407-6427.

[16] You, Q., Shi, Z.Y. and Law, S.S. (2011). Comparative studies of computation tools for moving force identification. *Journal of Vibration Engineering*. **13**(3): 487-504.

[17] Law, S.S. and Fang, Y.L. (2001). Moving force identification: optimal state estimation approach. *Journal of Sound and Vibration*, **239**(2): 233-54.

[18] Busby, H.R. and Trujillo, D.M. (1987). Solution of an inverse dynamics problem using an eigenvalue reduction technique. *Computers and Structures*, **25**(1): 109-17.

[19] Rubinstein, R.Y. and Kroese, D.P. (2004). *The cross-entropy method*, Springer, New York, NY, USA.

[20] MatLab (2003). The MathWorks, Inc., MatLab, Version 6, USA. http://www.mathworks.com/

[21] Reddy, J.N. (1993). *An introduction to the Finite Element Method, 2nd Edition*, McGraw-Hill, New York, NY, USA.

[22] Zienkiewicz, O.C. and Taylor, R.L. (2000). *The finite element method*, 6th Edition, McGraw Hill, New York, NY, USA.

[23] El-Madany, M.M. (1988). Design optimization of truck suspensions using covariance analysis. *Computers & Structures*, **28**(2): 241-6.

[24] Green, M.F., Cebon, D. and Cole, D.J. (1995). Effects of vehicle suspension design on dynamics of highway bridges. *ASCE Journal of Structural Engineering*. **121**(2): 272-82.

[25] Kim, C.W., Kawatani, M. and Kim, K.B. (2005). Three-dimensional dynamic analysis for bridge-vehicle interaction with roadway roughness. *Computers and Structures*, **83**: 1627-45.

[26] Weaver, W. and Johnston, P.R. (1987). *Structural Dynamics by Finite Elements*, Prentice-Hall, Englewood Cliffs, UK.

[27] DIVINE (1997). *Dynamic interaction between vehicles and infrastructure experiment*. Organization for Economic Co-operation and Development. Available at: www.oecd.org/dataoecd/9/22/2754516.pdf (Accessed 28th June 2011).

[28] Cebon, D. and Newland, D.E. (1983). Artificial generation of road surface topography by the inverse F.F.T. method. *Vehicle System Dynamics*, **12**(1): 160-5.

[29] International Organization for Standardization ISO. (1995). *Mechanical vibration - Road surface profiles - Reporting of measure data, ISO 8608 (BS7853:1996)*.

[30] Harris, N.K., OBrien. E.J. and González, A. (2007). Reduction of bridge dynamic amplification through adjustment of vehicle suspension damping. *Journal of Sound and Vibration*, **302**(3): 471-85.

[31] Tikhonov, A.N. and Arsenin, V.Y. (1977). *Solutions of Ill-posed Problems*. Winston, New York, NY, USA.

[32] Busby, H.R. and Trujillo, D.M. (1997). Optimal regularization of an inverse dynamics problem. *Computers and Structures*, **63**(2): 243-8.

[33] Walsh, B.J. and González, A. (2009). Assessment of the Condition of a Beam Using a Static Loading Test. *Key Engineering Materials*, **413-414**: 269-76.

[34] Goldberg, D.E. (1989). *Genetic Algorithms in Search, Optimization and Machine Learning*. Addison-Wesley Publishing, Reading, MA, USA.

[35] de Boer, P., Kroese, D.P., Manor, S. and Rubinstein, R.Y. (2005). A Tutorial on the Cross-Entropy Method. *Annals of Operations Research*, **134**: 19-67.

[36] Botev, Z. and Kroese, D. (2004). Global likelihood optimization via the cross-entropy method, with an application to mixture models. . In: Ingalls, R.G., Rossetti, M.D., Smith, J.S. and Peters, H.A. (Eds.), *Proceedings of the 2004 Winter Simulation Conference, WSC*, Washington, DC, USA, 529-35.

[37] Kirkegaard, P.H., Nielsen, S.R.K. and Enevoldsen, I. (1997). *Heavy vehicles on minor highway bridges - Dynamic modelling of vehicles and bridges*. Aalborg University, Instituttet for Bygningsteknik.

[38] ARCHES program, Assessment and rehabilitation of central European Highway Structures (2009). *WP2: Structural Assessment and Monitoring*, EU 6th Framework, 2006-2009. Available at: http://arches.fehrl.org/ (Accessed 4th August 2011).

[39] OBrien, E.J. and Keogh, D. L. (1999). *Bridge deck Analysis*, E & FN Spon, London, UK.

[40] Rowley, C.W., OBrien, E.J., González, A. and Žnidarič, A. (2009). Experimental testing of a moving force identification bridge weigh-in-motion algorithm. *Experimental Mechanics*, **49(**5): 743-6.